

Hierarchically Divacancy Defect Building Dual-Activated Porous Carbon Fibers for High-Performance Energy-Storage Devices

Qing Wang, Fangyan Liu, Zeyuan Jin, Xiaoru Qiao, Haichao Huang, Xiang Chu, Da Xiong, Haitao Zhang, Yan Liu, and Weiqing Yang*

Renewable and environmentally friendly biomass-based carbon electrode materials naturally possess fast ion transport, high adsorption, and excellent chemical stability for high-performance energy-storage devices. However, intelligently building the effectively biomass-transferred carbon materials for the requirement of high energy density is still a big challenge to date. Here, a hierarchically divacancy defect building platform is reported for effectively biomass-transferred and highly interconnected 3D dual-activated porous carbon fibers (DACFs) based on the internal–external dual-activation function of the pre-embedded KOH and CO₂ molecular. This uniquely interconnected frameworks not only fully provide the abundant active sites for ion interaction, but also efficiently guarantee the substantial accommodation for ion storage. Based on this, the as-prepared DACFs-based supercapacitors deliver a high energy density of 61.3 Wh kg⁻¹ at a power density of 875 W kg⁻¹ in the EMIMBF₄ ionic liquid. This work not only provides a simple and efficient technique to enhance the energy density of carbon materials, but also probably promotes its additional application in environmental remediation.

1. Introduction

With the uninterrupted consumption of fossil energy and the substantial growth of energy demand, considerable progress has been made for exploring the new energy, such as solar,

Q. Wang, Dr. F. Liu, Z. Jin, X. Qiao, Dr. H. Huang, Dr. X. Chu, Dr. D. Xiong, Dr. H. Zhang, Dr. Y. Liu, Prof. W. Yang
Key Laboratory of Advanced Technologies of Materials, Ministry of Education

School of Materials Science and Engineering
Southwest Jiaotong University
Chengdu 610031, China
E-mail: wqyang@swjtu.edu.cn

Prof. W. Yang
State Key Laboratory of Traction Power
Southwest Jiaotong University
Chengdu 610031, China

Prof. W. Yang
Key Laboratory of Transportation Tunnel Engineering
Southwest Jiaotong University
Chengdu 610031, China

 The ORCID identification number(s) for the author(s) of this article can be found under <https://doi.org/10.1002/adfm.202002580>.

DOI: 10.1002/adfm.202002580

wind power, hydrogen energy, geothermal energy, tidal energy, and biomass energy.^[1–8] Among them, the renewable and available biomass energy has attracted more attention to substitute traditional energy, which is attributed to its advantages of the widespread sources and the sustainable environment.^[9–11] Despite these advantages, the porous carbon materials with low energy density still remains a huge challenge in practical application.^[12–14] Consequently, it is extremely important to explore simple and efficient technique to enhance the energy density of carbon materials.

In this regard, carbon materials, including carbon nanotubes, graphene, activated carbon (AC), and carbon aerogels, have been successfully prepared.^[15–18] However, due to the complex preparation process, poor environmental protection and high cost, it was extremely difficult to achieve large-scale commercialization

of supercapacitors. In particular, the preparation process of 2D graphene was not only complex and expensive, but also polluted the environment by chemical reagents.^[19–21] While the biomass-based carbon materials not only had the advantages of environmental protection and low cost, but also played a crucial role in solving the energy shortage.^[22,23] As far as biomass-based carbon materials were concerned, their energy storage characteristics were mainly determined by pore size distribution, specific surface area (SSA), and electronic structure.^[24]

The previously reported work confirmed that the AC with available SSA and suitable pore size distribution became the best electrode material for commercial supercapacitors.^[25] Therefore, the highly available SSA not only provided the abundant active sites for ion interaction, but also guaranteed the substantial accommodation for ion storage. While the suitable pore size distribution was not only conducive to the rapid transmission of electrolyte ions, but also beneficial to the effective contact between electrode materials and electrolyte ions. Based on this simple and efficient method, we had recently reported that the microporous carbon originated from the natural bio-waste miscellaneous wood fibers possessed highly available SSA and highly interconnected micropores.^[26]

Besides, the selection of biomass precursors also played an important role in the construction of porous carbon materials.

For instance, Yu et al. reported that biomass-based carbon fiber exhibited hierarchical pore size distribution and excellent electrochemical properties.^[27] Among them, the representative nanocellulose with the excellent wettability and the high porosity has been used as an important porous carbon electrode material and reinforcing materials in membranes or gel polymers or solid polymer electrolytes.

In this work, based on the rapidly grown and large-scale cultivated ramie as biomass raw materials, we design the highly interconnected 3D dual-activated porous carbon fibers (DACFs) by the divacancy-defect effect through the internal-external dual-activation function of the pre-embedded KOH and CO₂ molecular. In our strategy, KOH preferentially reacting with carbon connected to the -OH and CO₂ preemptively reacting with carbon on the -C-C- bonds can synergistically construct many divacancy defects for providing a large number of active sites. Therefore, this unique divacancy-defected structure provides a relatively high SSA and the suitable pore size distribution for high-performance energy-storage devices. As expected, the as-prepared DACFs-based

supercapacitors delivered a high power density of 875 W kg⁻¹ and a high energy density of 61.3 Wh kg⁻¹ simultaneously. We believed that this simple and efficient strategy can be useful for exploiting other porous carbon materials, and further promote their application in the field of biological systems and catalysis.

2. Result and Discussion

As shown in **Figure 1a**, the rapidly grown and large-scale cultivated ramie was employed to synthesize the porous carbon fibers by the divacancy-defect effect in which different types of carbon atoms internally-externally interact with pre-embedded KOH and CO₂ activated molecular, further forming the vacancy defects with a great deal of active sites (**Figure 1b**). The as-obtained DACFs showed highly interconnected 3D porous carbon fibers for facilitating the rapid transmission of electrolyte ions (**Figure 1c** and **Figure S1**, Supporting Information). Such unique porous carbon fibers could provide the abundant

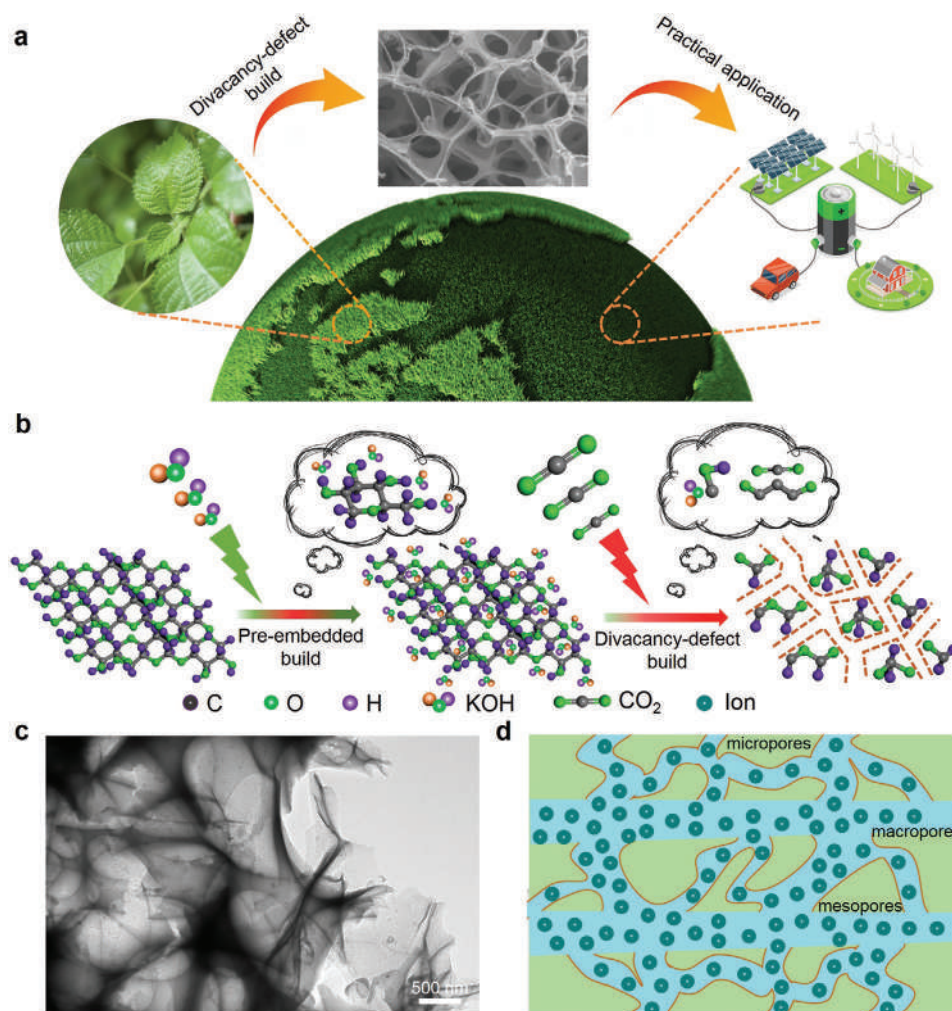


Figure 1. Rationally designing double activated carbon fibers (DACFs). a) The ramie with rapid growth and large-scale cultivation efficiently meet the demands of energy devices. b) Divacancy-defect effect of DACFs. c) Representative TEM image of DACFs. d) Schematic illustration of DACFs with suitable pore size distribution and substantial accommodation for ion storage.

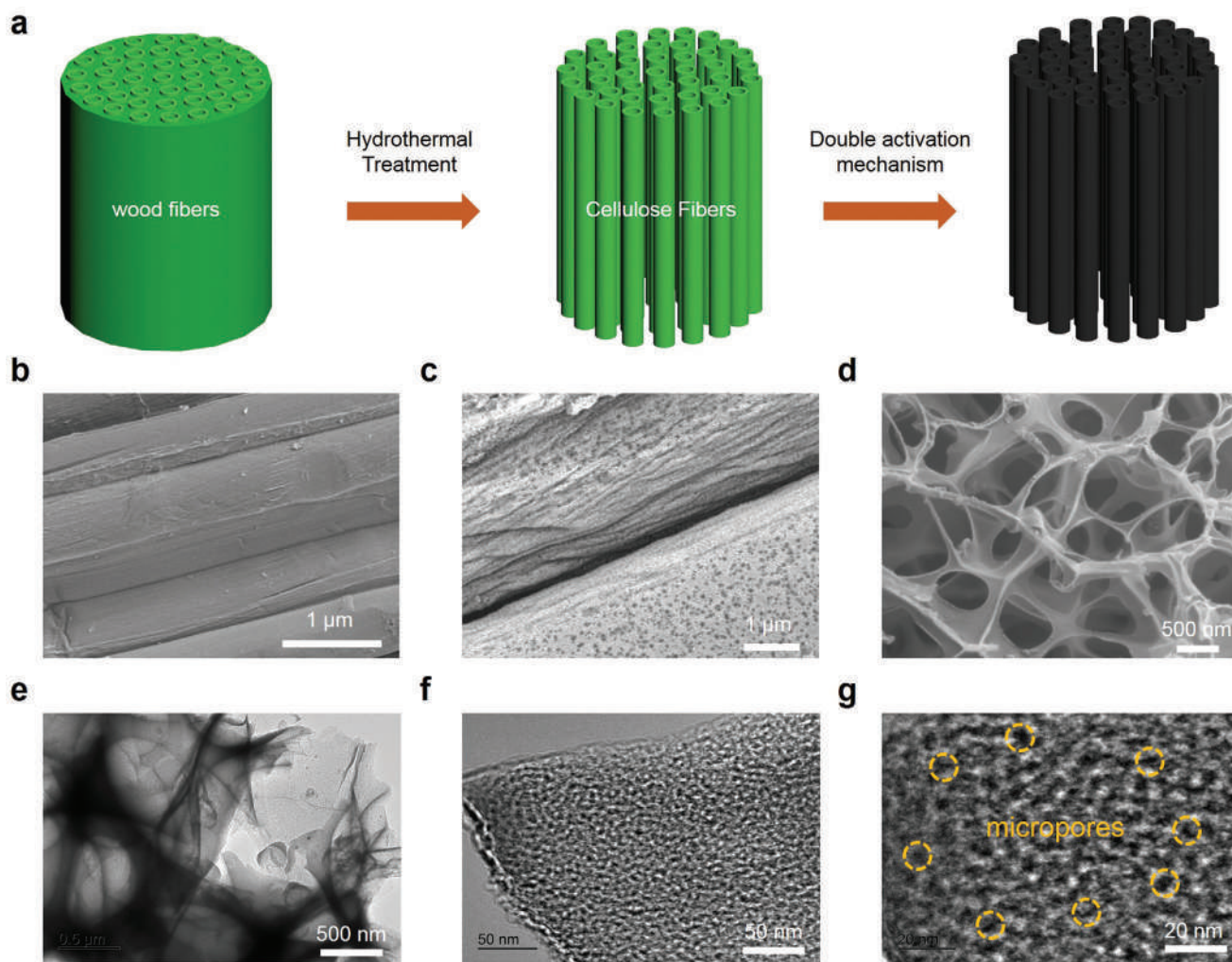


Figure 2. Preparation and morphology of double activated carbon fibers (DACFs). a) Schematic illustration for the synthesis of DACFs. b–d) SEM images of ramie fiber, ramie fiber-derived precursor, and DACFs, respectively. e) TEM images of DACFs at low magnification. f–g) High-resolution TEM images of DACFs with abundant microporous structure.

active sites for ion interaction and guarantee the substantial accommodation for ion storage (Figure 1d).

Figure 2a schematically illustrates the effectually building strategy of highly interconnected DACFs (more detailed information in the Experiment Section). First, the ramie with wide-spread sources and the sustainable environment (Figure 2b and Figure S2, Supporting Information) was used to prepare ramie fiber-derived precursor by hydrothermal carbonization of KOH solution for removing the lignin and hemicellulose. As shown in Figure 2c and Figure S3 (Supporting Information), this as-obtained precursor was obviously composed of large number of the tubular cellulose fibers. On the basis of precursor, the following generation of the porous carbon fibers was based on the reaction of the pre-embedded KOH and CO₂ molecular with carbon atoms on the precursor (Figure 2d and Figure S4, Supporting Information). In such unique structure, the interconnected framework could provide the abundantly ion-interacted active sites and guarantee the substantially ion-reserved accommodation for high-performance energy-storage devices such as supercapacitors.

To further investigate the microstructure of the as-prepared DACFs, the TEM images clearly revealed that the micromorphology of DACFs was formed by the accumulation of carbon nanosheets (Figure 2e). These carbon nanosheets apparently showed abundant microporous structure, which was mainly attributed to the divacancy mechanism and the removal of the impurities (Figure 2f,g). From the results of the EDS (Figure S5, Supporting Information), we further verified that the impurities were removed well in the DACFs. Meanwhile, XPS measurement further confirmed that the impurities were completely eliminated (Figure 3d). Remarkably, DACFs possessed a relatively high atomic percentage of carbon element ($\approx 96\%$) by comparing with oxygen element ($\approx 4\%$), and these terminated oxygen elements interacted with carbon as species of C–O and C–O–C groups (Figure 3e).

In order to illustrate the advantages of divacancy-defect effect, the surface physical measurements were characterized for determining the structural composition, chemical groups, structural defects, and crystallinity. As shown in Figure 3a, the Fourier transform infrared spectroscopy (FTIR) curve

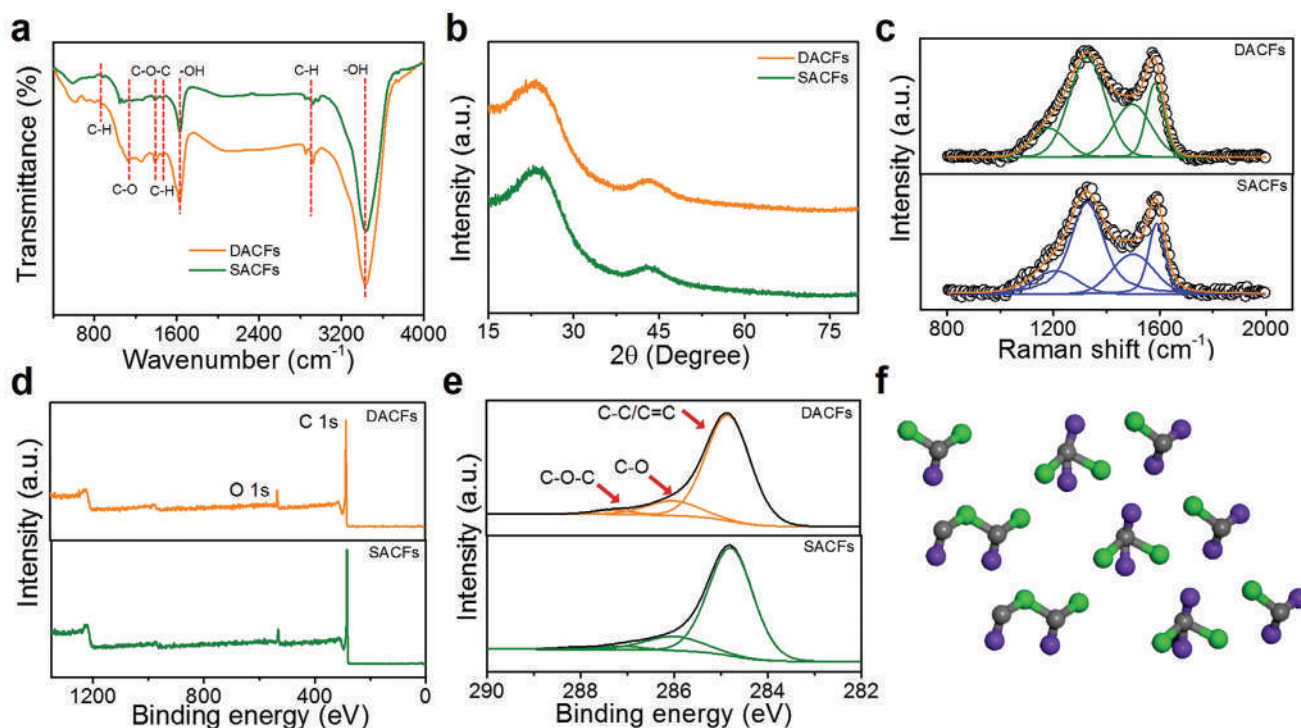


Figure 3. Physical characterization of double activated carbon fibers (DACFs) and single activated carbon fibers (SACFs). a) Fourier transform infrared spectroscopy (FTIR) curve. b) X-ray diffractometer (XRD) patterns. c) Raman spectrum. d) XPS survey. e) Deconvolution curves of C1s. f) Chemical bonds and functional groups of DACFs.

confirmed hydrogen-bonded O–H stretching vibration was located at 3353 and 1618 cm^{-1} . Then, the expansion vibration peak of $-\text{CH}_2$ group was situated at 2912 cm^{-1} . Finally, the peak around 1240 cm^{-1} was ascribed to the bending vibration peak of C–O–C. These results evidently indicated that chemical bonds and functional groups were extremely reasonable (Figure 3f). As shown in Figure 3b, the X-ray diffractometer (XRD) patterns of DACFs indicated that two broad (002) and (100) typical diffraction peaks were approximately located at $2\theta = 23.7^\circ$ and 43.3° , respectively. Obviously, the significant intensity of (002) diffraction peaks indicated the enhancement of the nongraphitic structure by the increment of pre-embedded KOH concentration. Also, the Raman spectrum was characterized for implying the structural defects of the DACFs (Figure 3c). Through calculating the area of D-band (1350 cm^{-1}) and G-band (1590 cm^{-1}) by using four peaks fit through Voigt function, the intensity ratio of I_D/I_G for the DACFs and SACFs were 2.69 ± 0.02 and 2.59 ± 0.03 , respectively, which further proclaimed more defects of the DACFs.

After understanding the divacancy-defect effect of DACFs, the as-prepared DACFs with abundant microporous structure and suitable pore size distribution had high expectations as an excellent electrode material for high-performance energy-storage devices such as supercapacitors. On the one hand, the galvanostatic charge/discharge (GCD) and cyclic voltammetry (CV) were used to characterize the electrochemical performance in a three-electrode configuration with 6.0 M KOH electrolyte (Figure S6, Supporting Information). On the other hand, we fabricated the symmetrical supercapacitors with 6 M KOH electrolyte for considering the electrochemical properties of

DACFs. As shown in Figure 4a, the Nyquist plots were used to obtain the information of solution resistance (R_s), double layer capacitance (C_d), and charge transfer resistance (R_{ct}) in different frequency ranges. Particularly, the vertical line indicated a good electric double layer capacitance in the low frequency region. While the Warburg regain implied a rapid ionic diffusion in the high frequency region (Figure 4a). Then, the CV curves exhibited a rectangular shape at a scan rate of 50 mV s^{-1} for indicating an ideal electric double layer capacitance (Figure 4b). While the GCD curves showed a triangle shape at a current density of 0.5 A g^{-1} for demonstrating the excellent rate capability (Figure 4c and Figure S7, Supporting Information). Interestingly, the specific capacitance is 53 F g^{-1} (212 F g^{-1} for a single electrode) at 0.5 A g^{-1} . Even at 20 A g^{-1} , it exhibited an excellent specific capacitance retention of 65% (Figure 4d). With increasing the scanning rate of 500 mV s^{-1} , the CV curve still showed an excellent rectangular shape for indicating an ideal capacitance characteristic (Figure 4e).

As shown in Figure 4f, the Ragone plots of the as-prepared DACFs-based supercapacitors with 6 M KOH electrolyte delivered a high power density of 0.25 kW kg^{-1} and a high energy density of 7.36 Wh kg^{-1} simultaneously. As the power density dramatically increased by 3900%, its energy density still maintained outstanding capability retention of 4.72 Wh kg^{-1} . These results were much better than the previously reported porous carbon-based supercapacitors. To further illustrate the electrochemical properties of the supercapacitors, the series and parallel test was used to evaluate the device integration for demonstrating the application potential (Figure 4g,h). Moreover, the DACFs possessed a relatively high capacitance retention of 96%

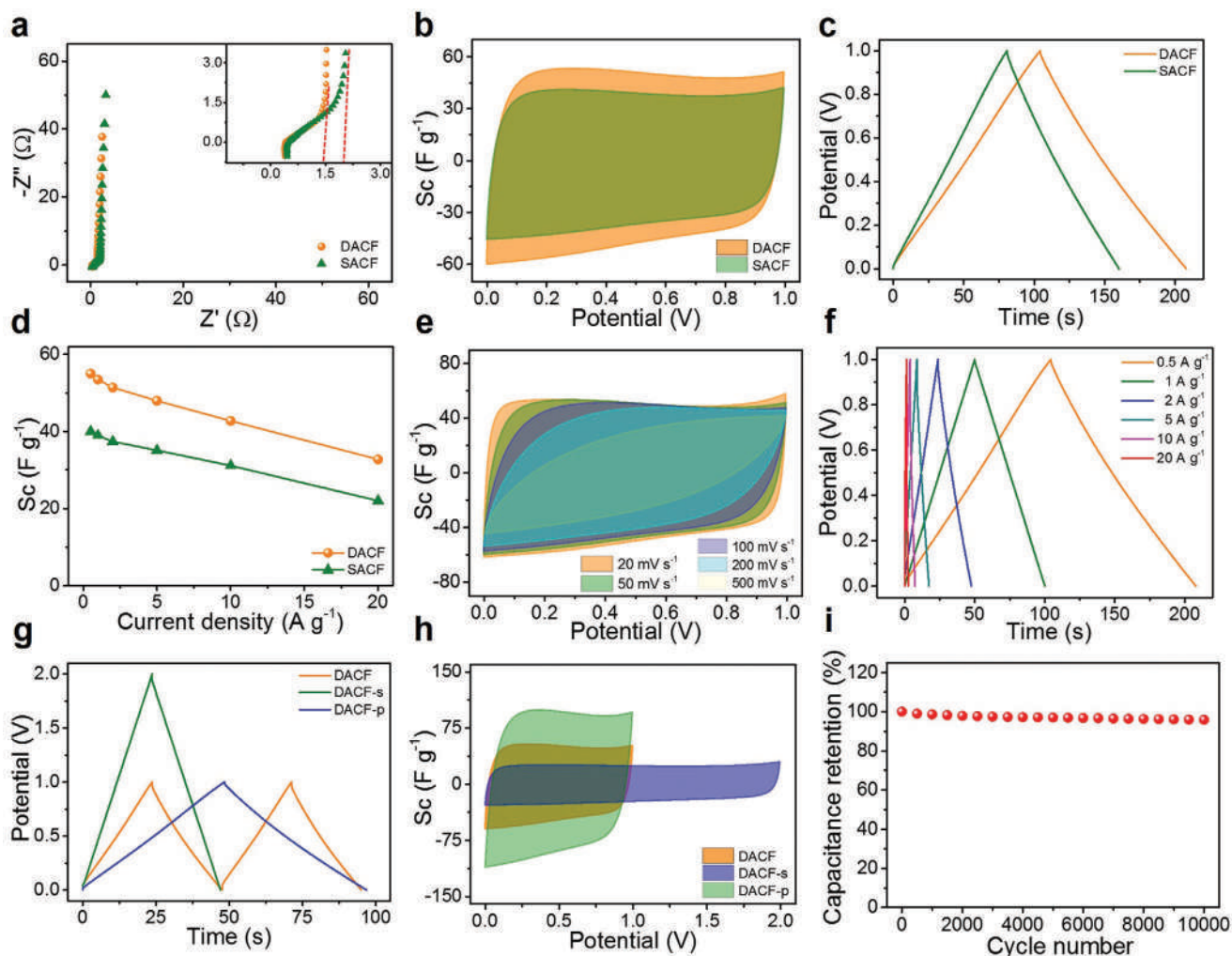


Figure 4. The electrochemical properties of double activated carbon fibers (DACFs) based symmetrical supercapacitors in 6 m KOH electrolyte. a) Nyquist plots. b) Cyclic voltammetry (CV) curves at the scan rate of 50 mV s^{-1} . c) Galvanostatic charge/discharge (GCD) curves at the current density of 0.5 A g^{-1} . d) The mass specific capacitance at different current densities. e) CV curves at the different scan rates of 20–500 mV s^{-1} . f) GCD curves at the different current density of 0.5–20 A g^{-1} . g) GCD curves at the current density of 2 A g^{-1} and h) CV curves at the scan rate of 50 mV s^{-1} for comparing the single device (orange), two devices interconnected in parallel (olive) and serial (blue). i) Cycling stability of DACFs at a current density of 2 A g^{-1} .

after 10 000 cycles at a current density of 2 A g^{-1} for implying the remarkable cycling stability (Figure 4i). In addition, the contact angle tests were used to characterize the hydrophilic of DACFs. Obviously, with the development of the divacancy-defect effect, the doping ability of the oxygen atoms was weakened, which caused the hydrophobicity of the DACFs (Figure S8, Supporting Information).

To further explore the electrochemical characteristics of DACFs, the symmetrical supercapacitors were assembled in EMIMBF₄ ionic liquid electrolyte with a relatively high voltage window of 3.5 V. As shown in Figure 5a and Figure S9 (Supporting Information), all isotherms were confirmed to be the typical type IV for indicating the hierarchical porous carbon structures with micropores and mesopores. Especially, the DACFs exhibited wide pore distribution and possessed high SSA of $1529 \text{ m}^2 \text{ g}^{-1}$ by the DFT method (Figure 5b). Due to the hierarchical structure and porous nature, the specific capacitance was 38.2 F g^{-1} at 0.5 A g^{-1} (Figure 5c). Interestingly, the

CV curves showed a nearly ideal rectangular shape at a scan rate of 50 mV s^{-1} for indicating an ideal electric double layer capacitance (Figure 5d). While the GCD curves exhibited a triangle shape at a current density of 1 A g^{-1} for demonstrating the excellent rate capability (Figure 5e). With increasing the scanning rate of 500 mV s^{-1} , the CV curve still showed an excellent rectangular shape for indicating an ideal capacitance characteristic (Figure 5g). As shown in Figure 5h, the Ragone plots of DACFs-based supercapacitors clearly delivered an energy density of 875 W kg^{-1} and a power density of 61.3 Wh kg^{-1} . Moreover, the DACFs possessed a relatively high capacitance retention of 85% after 10 000 cycles at a current density of 2 A g^{-1} for implying the remarkable cycling stability (Figure 5i).

The outstanding results of electrochemical properties could be attributed to the combination of abundant active sites and suitable pore size distribution for solving the difficulties of ion transport. First, the porous carbon fibers were synthesized by the divacancy-defect effect through the internal–external

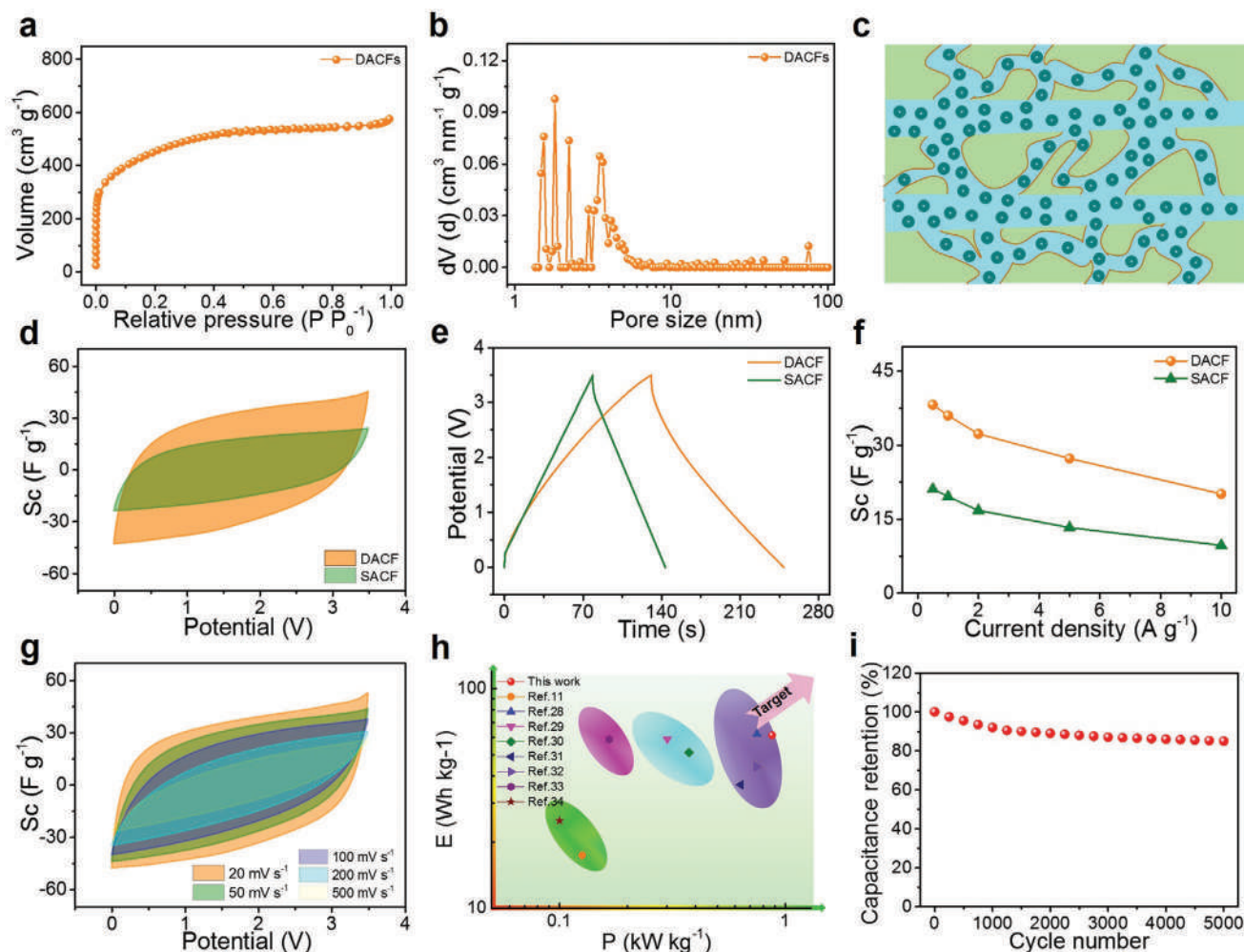


Figure 5. The electrochemical properties of double activated carbon fibers (DACFs) based symmetrical supercapacitors in EMIMBF₄ ionic liquid electrolyte. a) N₂ adsorption/desorption isotherms of DACFs and single activated carbon fibers (SACFs). b) Pore size distribution obtained by density functional theory (DFT) method. c) The mass specific capacitance at different current densities. d) Cyclic voltammetry (CV) curves at the scan rate of 50 mV s⁻¹. e) Galvanostatic charge/discharge (GCD) curves at the current density of 1 A g⁻¹. f) Schematic illustration of DACFs with suitable pore size distribution and substantial accommodation for ion storage. g) CV curves at the different scan rates of 20–500 mV s⁻¹. h) Ragone Plots of the power density and energy density of DACFs in comparison with other carbon materials in EMIMBF₄ ionic liquid electrolyte.^[11,28–34] i) Cycling stability of DACFs at a current density of 2 A g⁻¹.

dual-activation function of the pre-embedded KOH and CO₂ molecular for making full use of the difference of reaction principle, further forming the vacancy defects. Then, the suitable pore size distribution of DACFs with the abundantly ion-interacted active sites and the substantially ion-reserved accommodation increased the available SSA to form the electric double-layer capacitance. More importantly, the divacancy-defect effect not only provides a simple and efficient technique to enhance the energy density of carbon materials, but also probably promotes its extended application in biological systems and catalysis.

3. Conclusion

In conclusion, we demonstrated a hierarchically divacancy defect building platform for effectively biomass-transferred

and highly interconnected DACFs through the internal-external dual-activation function of the pre-embedded KOH and CO₂ molecular by using the rapidly grown and large-scale cultivated ramie as biomass raw materials. Results showed that these unique vacancy structures not only exhibited a relatively high SSA of 1529 m² g⁻¹, but also built suitable pore size distribution, further effectively creating abundantly ion-interacted active sites and effectually providing substantially ion-reserved accommodation. Further, the as-prepared DACFs-based supercapacitors with EMIMBF₄ ionic liquid deliver a power density of 875 W kg⁻¹ and a high energy density of 61.3 Wh kg⁻¹ simultaneously. Evidently, these promising results explicitly confirm that the divacancy construction of porous carbon fibers not only solves the problem of ion transport of energy-storage devices, but also promotes its potential applications in biological systems and catalysis.

4. Experimental Section

Preparation of Ramie Fiber-Derived Precursor: The precursors were synthesized by hydrothermal carbonization of the ramie fiber. First, the 1 g ramie fiber was evenly dispersed in 25 mL of different concentrations (1–6 M) of KOH solution (Chengdu Kelong Chemicals Co., Ltd., China) and then transferred to a 50 mL high temperature reactor. After that, the reactor was placed in an oven and heated up to 150 °C for 6 h. After naturally cooling to room temperature, the as-prepared precursors were washed repeatedly with abundant deionized water for removing the impurities (lignin and hemi-cellulose) from the precursors surface, and dried at 60 °C for 12 h.

Preparation of Single Activated Carbon Fibers (SACFs): The SACFs were synthesized by a simple method of carbon atom reaction with KOH. First, the precursors were put into a tube furnace (GSL-1700X, Hefei Kejing Materials Tech. CO., Ltd., China) with a multichannel flow controller (GMF-2Z, AnHui BEQ Equipment Tech. CO., Ltd. China). After that, the precursors were heated to the reactive temperature (700 °C) at a heating rate of 4 °C min⁻¹ under Ar atmosphere (40 sccm) for 60 min. Finally, waiting for the tubular furnace to cool naturally to the room temperature over 8 h, the as-prepared samples were taken out and put them into a beaker with 1 M HCl solution to remove the residual KOH for 12 h, washed repeatedly with a large amount of deionized water and alcohol, and dried at 60 °C for 12 h. According to the activation mechanism, the as-prepared samples were denoted as SACFs.

Preparation of Double Activated Carbon Fibers (DACFs): The DACFs were synthesized by an efficient method of carbon atom reaction with KOH and CO₂. In a typical procedure, the precursors went up to the aimed reaction temperature (700 °C) under the protection of Ar gas with a flow rate of 40 sccm (GMF-2Z, AnHui BEQ Equipment Tech. CO., Ltd. China) in the tube furnace (GSL-1700X, Hefei Kejing Materials Tech. CO., Ltd., China), the same ratio of CO₂ to Ar was continuously introduced for 1 h. When the temperature of the tube furnace cooled naturally over 8 h, the obtained samples were treated with 1 M HCl solution for eliminating the impurities at room temperature for 12 h. Then, the as-prepared products were washed repeatedly with a large amount of deionized water and alcohol, and dried at 60 °C for 12 h. According to the activation mechanism, the as-prepared samples were denoted as DACFs.

Characterization Methods: The scanning electron microscope (JEOL JSM-7800 Prime) and transmission electron microscope (JEOL JEM-2100F) with an accelerating voltage of 5 kV were used to characterize the micromorphologies of the samples. X-ray diffractometer (XRD) patterns were obtained to determine the basic phase and composition using a PANalytical X'Pert powder (wavelength 0.15406 nm) with Cu K α source and 2 θ range from 10° to 80°. Energy dispersive X-ray spectrometer (JEOL JSM-7800 Prime) and X-ray photoelectron spectroscopy (Thermo Scientific ESCALAB 250Xi) were recorded to determine the basic composition. The Brunauer–Emmett–Teller (BET) surface areas and density functional theory (DFT) pore size distribution measurements of SACFs and DACFs powers were characterized by Micromeritics ASAP 2020 surface area and pore size analyzer using N₂ adsorption/desorption isotherm at -196 °C, respectively. Raman spectrum was measured by RM2000 microscopic confocal Raman spectrometer employing a 514 nm laser beam for determining the defects state of carbon materials. Fourier transform infrared spectroscopy (FTIR) patterns were obtained to determine the types and changes of functional groups in materials using a TENSOR II spectrometer (Bruker) with a spectral resolution of 4 cm⁻¹ at a scanning frequency of 1 spectrum min⁻¹. The contact angle test (Dataphysics DSA100 contact-angle system) was used to characterize the wettability of DACFs.

The electrodes of supercapacitors were prepared by DACFs, conductive additive (Super C45, Timical), and PTFE (Sigma–Aldrich) with a mass ratio of 80:10:10. After adding the isopropyl alcohol (Sigma–Aldrich) into the weighing bottle and stirring evenly, the compact dough was punched into a very thin piece of wafer with a diameter of 8 mm and a thickness of 100 μ m by a punching machine. Then, the polypropylene paper separator was sandwiched into two DACFs electrodes that fully

wetted by EMIMBF₄ ionic liquid electrolyte or 6 M KOH solution for the CR2032 coin-type cells. Particularly, when the EMIMBF₄ ionic liquid was used as the electrolyte, the packaging process was carried out in the glove box (Unilab Plus, Mbraun, Germany, H₂O < 0.1 ppm, O₂ < 0.1 ppm). After that, CV, EIS, and GCD tests were conducted on a CHI660E electrochemical workstation (Chenhua, Shanghai, China). The cycling lifetime test was measured on an Arbin MSTAT4 multichannel galvanostat/potentiostat instrument.

Supporting Information

Supporting Information is available from the Wiley Online Library or from the author.

Acknowledgements

W.Y. acknowledged the National Natural Science Foundation of China (Nos. 51977185, 51972277, 51602265), the Sichuan Science and Technology Program (No. 2018RZ0074), the Cultivation Program for the Excellent Doctoral Dissertation of Southwest Jiaotong University (No. D-YB201709), and the Analytical and Testing Center of Southwest Jiaotong University for supporting the SEM and TEM measurements. The authors also gratefully acknowledge the ceshigo (www.ceshigo.com) for providing testing services.

Conflict of Interest

The authors declare no conflict of interest.

Keywords

abundant active sites, energy density, energy-storage devices, interconnected micropores, substantial accommodation

Received: March 21, 2020

Revised: May 19, 2020

Published online:

- [1] J. X. Zhao, B. Wang, Q. Zhou, H. B. Wang, X. H. Li, H. Y. Chen, Q. Wei, D. Wu, Y. L. Luo, J. M. You, F. (F) Gong, X. P. Sun, *Chem. Commun.* **2019**, 55, 4997.
- [2] T. S. Blankenship, R. Mokaya, *Energy Environ. Sci.* **2017**, 10, 2552.
- [3] W. F. Chen, S. Iyer, S. Iyer, K. Sasaki, C. H. Wang, Y. M. Zhu, J. T. Muckerman, E. Fujita, *Energy Environ. Sci.* **2013**, 6, 1818.
- [4] L. Wang, Y. T. Shi, Y. X. Wang, H. Zhang, H. W. Zhou, Y. Wei, S. Y. Tao, T. L. Ma, *Chem. Commun.* **2014**, 50, 1701.
- [5] Q. L. Ma, Y. F. Yu, M. Sindoro, A. G. Fane, R. Wang, H. Zhang, *Adv. Mater.* **2017**, 29, 1605361.
- [6] J. Z. Chen, K. L. Fang, Q. Y. Chen, J. L. Xu, C. P. Wong, *Nano Energy* **2018**, 53, 337.
- [7] M. L. Kong, Z. Wang, W. Y. Wang, M. Ma, D. N. Liu, S. Hao, R. M. Kong, G. Du, A. M. Asiri, Y. D. Yao, X. P. Sun, *Chem. - Eur. J.* **2017**, 23, 4435.
- [8] S. M. Xu, X. Liang, X. Y. Wu, S. L. Zhao, J. Chen, K. X. Wang, J. S. Chen, *Nat. Commun.* **2019**, 10, 5810.
- [9] J. W. Lee, B. Hawkins, D. M. Day, D. C. Reicosky, *Energy Environ. Sci.* **2010**, 3, 1695.
- [10] Z. L. Wang, T. Jiang, L. Xu, *Nano Energy* **2017**, 39, 9.

- [11] L. Xia, J. J. Yang, H. B. Wang, R. B. Zhao, H. Y. Chen, W. H. Fang, A. M. Asiri, F. Y. Xie, *Chem. Commun.* **2019**, 55, 3371.
- [12] J. S. Wei, C. Ding, P. Zhang, H. Ding, X. Q. Niu, Y. Y. Ma, C. Li, Y. G. Wang, H. M. Xiong, *Adv. Mater.* **2018**, 31, 1806197.
- [13] W. H. Zuo, R. Z. Li, C. Zhou, Y. Y. Li, J. L. Xia, J. P. Liu, *Adv. Sci.* **2017**, 4, 1600539.
- [14] N. Choudhary, C. Li, J. Moore, N. Nagaiyah, L. Zhai, Y. Jung, J. Thomas, *Adv. Mater.* **2017**, 29, 1605336.
- [15] L. Yao, Q. Wu, P. X. Zhang, J. M. Zhang, D. R. Wang, Y. L. Li, X. Z. Ren, H. W. Mi, L. B. Deng, Z. J. Zheng, *Adv. Mater.* **2018**, 30, 1706054.
- [16] J. X. Zhao, J. J. Yang, L. Ji, H. B. Wang, H. Y. Chen, Z. G. Niu, Q. Liu, T. S. Li, G. L. Cui, X. P. Sun, *Chem. Commun.* **2019**, 55, 4266.
- [17] J. Y. Luo, H. D. Jang, J. X. Huang, *ACS Nano* **2013**, 7, 1464.
- [18] J. Biener, M. Stadermann, M. Suss, M. A. Worsley, M. M. Biener, K. A. Rose, T. F. Baumann, *Energy Environ. Sci.* **2011**, 4, 656.
- [19] J. X. Zhang, Z. Z. Zhang, Y. T. Jiao, H. X. Yang, Y. Q. Li, J. Zhang, P. Gao, *J. Power Sources* **2019**, 419, 99.
- [20] H. H. Cheng, Y. Hu, F. Zhao, Z. L. Dong, Y. H. Wang, N. Chen, Z. P. Zhang, L. T. Qu, *Adv. Mater.* **2014**, 26, 2909.
- [21] L. Wang, H. K. Bisoyi, Z. G. Zheng, K. G. Gutierrez-Cuevas, G. Singh, S. Kumar, T. J. Bunning, Q. Li, *Mater. Today* **2017**, 20, 230.
- [22] J. Chen, Y. Huang, N. N. Zhang, H. Y. Zou, R. Y. Liu, C. Y. Tao, X. Fan, Z. L. Wang, *Nat. Energy* **2016**, 1, 16138.
- [23] F. Y. Liu, Z. X. Wang, H. T. Zhang, L. Jin, X. Chu, B. N. Gu, H. C. Huang, W. Q. Yang, *Carbon* **2019**, 149, 105.
- [24] B. N. Gu, H. Su, X. Chu, Q. Wang, H. C. Huang, J. Q. He, T. J. Wu, W. L. Deng, H. T. Zhang, W. Q. Yang, *Chem. Eng. J.* **2019**, 361, 1296.
- [25] J. Chen, Z. L. Wang, *Joule* **2017**, 1, 480.
- [26] F. Y. Liu, X. Chu, H. T. Zhang, B. B. Zhang, H. Su, L. Jin, Z. X. Wang, H. C. Huang, W. Q. Yang, *Electrochim. Acta* **2018**, 269, 102.
- [27] G. F. Shi, C. Liu, G. Y. Wang, X. F. Chen, L. Li, X. Jiang, P. Zhang, Y. C. Dong, S. M. Jia, H. Q. Tian, Y. R. Liu, Z. Wang, Q. Zhang, H. Q. Zhang, *Ionics* **2019**, 25, 1805.
- [28] W. H. Yu, H. L. Wang, S. Liu, N. Mao, X. Liu, J. Shi, W. Liu, S. G. Chen, X. Wang, *J. Mater. Chem. A* **2016**, 4, 5973.
- [29] B. Duan, X. Gao, X. Yao, Y. Fang, L. Huang, J. Zhou, L. N. Zhang, *Nano Energy* **2016**, 27, 482.
- [30] H. L. Wang, Z. Li, J. K. Tak, C. M. B. Holt, X. H. Tan, Z. W. Xu, B. S. Amirkhiz, D. Hayfield, A. Anyia, T. Stephenson, D. Mitlin, *Carbon* **2013**, 57, 317.
- [31] X. Wang, C. X. Lu, H. F. Peng, X. Zhang, Z. K. Wang, G. K. Wang, *J. Power Sources* **2016**, 324, 188.
- [32] Y. P. Cui, H. L. Wang, N. Mao, W. H. Yu, J. Shi, M. H. Huang, W. Liu, S. G. Chen, X. Wang, *J. Power Sources* **2017**, 361, 182.
- [33] W. Q. Tian, Q. M. Gao, Y. L. Tan, K. Yang, L. H. Zhu, C. X. Yang, H. Zhang, *J. Mater. Chem. A* **2015**, 3, 5656.
- [34] Z. Li, J. Liu, K. R. Jiang, T. Thundat, *Nano Energy* **2016**, 25, 161.